Passive Stability of Vehicles Without Angular Momentum Including Quadrotors and Ornithopters

Matthew Piccoli[1] and Mark Yim[2]

***Abstract*— The paper presents a model for adding stabilizers to a flying device without rotational momentum (such as quadrotors or ornithopters) that will create passively stable vehicles in hover. This model enables the design of the size and location of these stabilizers that will vary the stability and performance of the vehicle. The model is verified with nine experimental vehicles that span the stability design space. Passive stability allows the removal of costly inertial sensors and increases the robustness of the vehicle. Analysis of the cost and drag that impacts flight performance is also discussed.**

I. INTRODUCTION

There has been an increasing interest in micro air vehicles (MAVs). These robotic air vehicles can hover and be arbitrarily positioned in 3D space. The applications range from search and rescue of hazardous or unreachable locations to delivery of payloads and most recently to toys. Simple, low-cost MAVs could also democratize the use of these devices and fit many consumer applications including robotic information aids and personal assistants.

Four-propeller MAVs, called quadrotors or quadcopters, are becoming popular as seen by commercially available devices for the consumer market. The stability of these vehicles is not trivial, but now can be considered a solved problem - as evidenced by the available commercial devices [1] [2] [3]. To do this, inertial sensors must estimate the vehicle's orientation and a closed-loop controller must actuate the rotors to lead to stable hover and flight.

If the MAVs had *passive* stability, they would not require expensive inertial sensors nor active closed-loop control to keep from crashing. While inertial sensors and microcontrollers have become much cheaper, enabling the current explosion in commercially available quadrotors, they still remain the most expensive components in small quadrotors as will be shown. Passive stability would lower the cost and also make them more robust to control failures, such as bad data from sensors, control software, or damaged actuators. Furthermore, many MAVs already have protection cages, which could double as stabilizers [4].

Passively stabilized flying vehicles have been around for many years. For example, some full sized helicopters have flybars or paddles and some airplanes use wing dihedral and tail horizontal and vertical stabilizers. The helicopter stabilizers are *inertial*, in that they reference inertia (via gyroscopes), while the airplane stabilizers are *aerodynamic* and reference the surrounding air. When hovering vehicles are aerodynamically stabilized, they are hovering with respect to the wind around them whether the air is stationary, like indoors, or moving at high velocities.

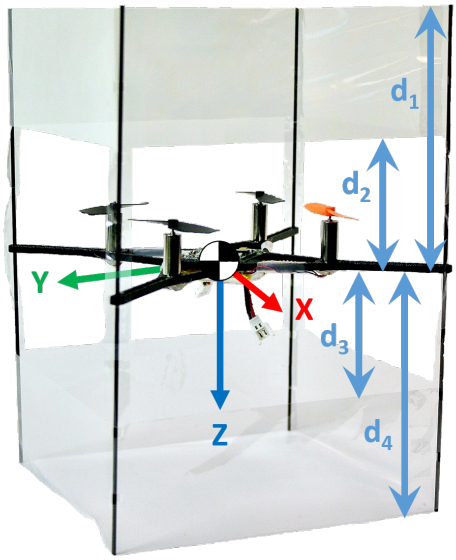

Fig. 1: Prototype test platform.

Recognizing that cost is the most important concern, most manufacturers of toy helicopters have adopted these techniques, simplifying control as well. They have also scaled down these mechanisms to MAVs on the order of tens of grams. Most of these MAVs omit the actuators and mechanisms for roll and/or pitch control in order or reduce size and weight, yet the passive stabilizers are able to keep the vehicle upright [5] [6]. Some of the disadvantages of adding passive stabilizers include the increased mass from the stabilizers and the power cost when operating away from the stable state. In related work by the authors [5], two classes of aerodynamic passive stability for hovering vehicles were identified, one for vehicles with large angular momentum and one for vehicles with no net angular momentum. This past work focused on rotorcraft with net angular momentum. This paper focuses on vehicles with little net angular momentum, which includes even numbered multirotor vehicles such as quadrotors, coaxial helicopters, and tandem helicopters, as well as ornithopters, like the robobee, and hovering rockets [6]. It is important to distinguish between these two classes, specifically focusing on angular momentum, as they emphasize conflicting design parameters.

[1]Matthew Piccoli is a Ph.D. student of Mechanical Engineering and Applied Mechanics, University of Pennsylvania, Philadelphia, PA 19104, USA piccoli@seas.upenn.edu

[2]Mark Yim with the Department of Mechanical Engineering and Applied Mechanics, University of Pennsylvania, Philadelphia, PA 19104, USA yim@seas.upenn.edu

The authors would like to acknowledge the support of NSF grant CCF-1138847.

The essential property for aerodynamic stability in hover in the no angular moment case is to have the center of pressure (COP) in horizontal flow above the center of mass (COM), or COP $>$ COM. Emphasizing this property in a vehicle with large angular moment destabilizes the system.

Other vehicles have used this COP $>$ COM principle in flapping wing devices [6] [7]. In these cases, passive drag sails were placed above and below the vehicle and were developed to help stabilize the vehicle; however, design parameters (e.g. size and location of the drag sails) were not extensively analyzed. Other systems could benefit from COM $>$ COM stabilization, such as low altitude weather monitoring devices, indoor draft detection, and safe yet low cost indoor fly toys.

II. VEHICLE DESCRIPTION

The generic requirements for this system is a vehicle that can create thrust while hovering with no net angular momentum. In our case, we attach stabilizers, sometimes called dampers or drag sails, to a quadrotor. Typically, one stabilizer is above the COM and a second is below the COM. See Fig. 1 as a reference. The top stabilizer provides the desired COP $>$ COM moment, which restores the vehicle's attitude to vertical. The bottom stabilizer is added to increase the effective damping by both increasing linear and angular damping as well as reducing the net COP $>$ COM moment.

If both the top and bottom stabilizer are the same size, shape, and distance from the COM, then the COP $=$ COM, there is no restoring moment (ignoring effects from the vehicle itself), and the stabilizers are purely linear and angular dampers. Net forces from rotating are eliminated when the top and bottom plates are well matched. Although uncommon, a single, well sized top stabilizer can provide both the COP $>$ COM moment and sufficient damping. The below algorithms are capable of finding such configurations.

A. Vehicle Dynamics

Much of the notation and equations are taken from [8], which defines u, v, w, p, q, r as the X, Y, Z linear and angular velocities in the body frame. ϕ, θ, ψ are the X, Y, Z world to body Euler angles. X, Y, Z, L, M, N are the X, Y, Z forces and moments in the body frame. When a force is subscripted by a velocity it becomes an acceleration sensitivity. For example, $X_u = \frac{\partial X}{m \partial u}$ or $L_q = \frac{\partial L}{I_{XX} \partial q}$.

In [5], a linear time invariant (LTI) model with small angle approximations of a flying vehicle constrained to a horizontal plane, such as an altitude controlled MAV, is:

$$\begin{bmatrix} \dot{u} \\ \dot{v} \\ \dot{p} \\ \dot{q} \\ \dot{\phi} \\ \dot{\theta} \end{bmatrix} = \begin{bmatrix} X_u & X_v & X_p & X_q & 0 & -g \\ Y_u & Y_v & Y_p & Y_q & g & 0 \\ L_u & L_v & L_p & L_q & 0 & 0 \\ M_u & M_v & M_p & M_q & 0 & 0 \\ 0 & 0 & 1 & 0 & 0 & 0 \\ 0 & 0 & 0 & 1 & 0 & 0 \end{bmatrix} \begin{bmatrix} u \\ v \\ p \\ q \\ \phi \\ \theta \end{bmatrix} \quad (1)$$

Because the vehicle is symmetric about the XZ plane and YZ plane, $X_u = Y_v$, $X_v = -Y_u$, $X_p = Y_q$, $X_q = -Y_p$, $L_u = M_v$, $L_v = -M_u$, $L_p = M_q$, and $L_q = -M_p$. Furthermore, this symmetry leads to $X_v = -Y_u = 0$ and $X_p = Y_q = 0$. L_u and M_v are generally caused by differential lift on propellers, which we assume to either be zero or cancel with all of the other propellers, as is the case with quadrotors. L_q and M_p are frequently the result of gyroscopic precession. Again, we assume the vehicle's net angular momentum is zero so that no precession occurs. The last two simplifications are not true for the vehicles mentioned in [5]. X_q and Y_p go to zero for vehicles whose stabilizers create a pure moment when rotated. We assume this is the case, although it is not guaranteed, and more exotic designs would benefit from leaving in these terms. We keep the remaining coefficients. X_u and Y_v represent linear drag. L_v and M_u are the rotational moments from linear motion and represent the COM vs COM interaction. L_p and M_q represent angular drag. We note that now u, q, and θ are dependent on each other, v, p, and ϕ are dependent on each other, and both sets are independent. We continue by examining linear x and angular y motion, noting that the system behaves identically in the linear y and angular x direction. The resulting linearized state equation becomes:

$$\begin{bmatrix} \dot{u} \\ \dot{q} \\ \dot{\theta} \end{bmatrix} = \begin{bmatrix} X_u & 0 & -g \\ M_u & M_q & 0 \\ 0 & 1 & 0 \end{bmatrix} \begin{bmatrix} u \\ q \\ \theta \end{bmatrix} \quad (2)$$

B. Vehicle Aerodynamics

We now need to fill in X_u, M_u, and M_q with our design parameters. We define drag as the force felt in the direction of wind and lift in the direction perpendicular to wind. Vehicles operating on pure drag assume that no wind from the thrust producing components of the vehicle blows across the stabilizers [6]. The coefficients generated by this method are significantly smaller than values extracted by test data with our vehicle.

For our vehicle, the inflow from the propellers create wind in the vertical, positive z direction. The vehicle's motion in the world creates the horizontal components of wind. Together, these two sources of wind create angles of attack of less than 10° from the z axis, which falls under both the linear region of the lift slope curve and the small angle approximation. Thus, the lift from this mechanism is linear with u motion and is felt along the x axis. Note that vertical motion also contributes to wind in the vertical direction, where rapid descents can cancel the propeller's inflow and the aerodynamics fall back to the lower magnitude drag equations. For the remainder of this discussion we assume there is no vehicle motion in the vertical direction. Furthermore, fluid flow through and around rotors is quite complicated and the analysis below is only a guideline.

Momentum theory states that $T = mg = 2\rho A_p \nu^2$ where T is thrust, m is the vehicle mass, g is the acceleration from gravity, ρ is surrounding air density, A_p is the propeller disc area, and ν is the inflow velocity. We assume $\nu >> u$ such that $\nu^2 + u^2 \approx \nu^2$ and $\arctan(\frac{u}{\nu}) \approx \frac{u}{\nu}$. Similarly, we assume $\nu >> qd$ where d is the distance between the center of mass and a stabilizer element. These assumptions hold for a limited flight envelope which is vehicle dependent and is discussed for a test vehicle in Section IV-A. We also include an adjustment term, $\beta = 0.5$, when computing the

wind velocity near the stabilizers to account for un-modeled aerodynamic effects and rotor-stabilizer proximity, resulting in $\nu = \sqrt{mg/(2\rho A_p)}\beta$.

The force generated by the stabilizers is $F = 1/2\rho\nu^2 A C_l(\alpha)$ where α is the angle of attack, $C_l(\alpha) = 2\pi\alpha$ is the coefficient of lift at a given angle of attack, and A is the area of the stabilizer element.

With $\alpha = \frac{-u}{\nu}$ and breaking A into the stabilizer width w and height d, X_u and M_u are:

$$\begin{aligned} X_u &= \rho\nu^2 w(\int_{d_1}^{d_2} \mathrm{d}d + \int_{d_3}^{d_4} \mathrm{d}d)2\pi(-u)/(2\nu m u) \\ &= \rho\nu w((d_1 - d_2) + (d_3 - d_4))\pi/m \end{aligned} \quad (3)$$

$$\begin{aligned} M_u &= \rho\nu^2 w(\int_{d_1}^{d_2} d\mathrm{d}d + \int_{d_3}^{d_4} d\mathrm{d}d)2\pi(-u)/(2\nu I u) \\ &= \rho\nu w((d_1^2 - d_2^2) + (d_3^2 - d_4^2))\pi/(2I) \end{aligned} \quad (4)$$

For angular rates, $\alpha = \frac{-dq}{\nu}$ and M_q is:

$$\begin{aligned} M_q &= \rho\nu^2 w(\int_{d_1}^{d_2} d^2\mathrm{d}d + \int_{d_3}^{d_4} d^2\mathrm{d}d)2\pi(-q)/(2\nu I q) \\ &= \rho\nu w((d_1^3 - d_2^3) + (d_3^3 - d_4^3))\pi/(3I) \end{aligned} \quad (5)$$

For higher fidelity, m and I should be a function of d_1, d_2, d_3, and d_4 as well.

III. STABILITY

Now that we can adequately describe our vehicle, we can begin our stability analysis. For our hovering vehicles, we define stability as having a bounded angle from vertical and a bounded velocity in response to a disturbance with an ultimate return to upright and no velocity. Smaller bounded angles and velocities are better. Active vehicle controllers sense the vehicle's state and manipulate actuators to correct its state. Passively stabilized vehicles do not possess a controller in the directions that are passively stabilized. For example, helicopters that have flybars are passively stable in roll and pitch, but require active yaw and altitude controllers. On human-scale helicopters with large time constants, the active controllers are the human pilots themselves.

A. Routh-Hurwitz Stability Criteria

The Routh-Hurwitz stability criterion is an efficient, necessary, and sufficient method for determining if an LTI of the form $\dot{x} = Ax$ is stable using its characteristic equation, $\det(A - \lambda I) = 0$. A third order characteristic polynomial has the form $a_3 s^3 + a_2 s^2 + a_1 s^1 + a_0$. The criteria states that if $a_3, a_2, a_1, a_0 > 0$ and $a_2 a_1 > a_3 a_0$ then the system is stable. The characteristic polynomial of Equation 2 is $s^3 - (X_u + M_q)s^2 + X_u M_q s + M_u g$. The combination of $a_2 = -(X_u + M_q) > 0$ and $a_3 = X_u M_q > 0$ requires that both $X_u < 0$ and $M_q < 0$. This makes sense since both of these terms represent drag, which is felt in the direction opposite to motion. The constraint $a_0 = M_u g > 0$ requires that $M_u > 0$ since g is positive (recall in our coordinate system z is down), which says that the net COP must be above (more negative than) the COM. Finally, $a_2 a_1 = -(X_u + M_q)X_u M_q > a_3 a_0 = 1 M_u g$ demands that $M_u < -(X_u + M_q)X_u M_q$, which we know is a positive number and is an aerodynamic damping requirement. This is the constraint of most interest because it puts an upper bound on the amount of COP > COM moment that the vehicle produces and is not frequently discussed [6] [7].

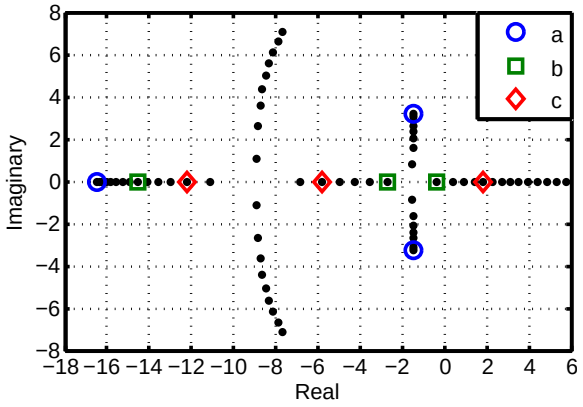

Fig. 2: Root locus varying d_2, holding $d_1 = -0.16\,\mathrm{m}$, $d_3 = 0.05\,\mathrm{m}$, $d_4 = 0.14\,\mathrm{m}$. Tested configurations are highlighted.

B. Root Locus

The Routh-Hurwitz stability criterion provides us important vehicle guidelines to make stable vehicles, but ultimately we want to know how stable. By computing the eigenvalues, λ, of our LTI, we can find time constants, τ, and damping ratios, ζ, of our vehicle. Our target is to find vehicles that are critically damped (damping ratios of one) so that our vehicle can have a fast and stable response to disturbances.

To design the desired stability we can explore the space of eigenvalues. Computers can quickly numerically calculate the eigenvalues of configurations. Once computed, we can search for parameters, including fastest response, least material, least linear drag, highest safety margin of stability, etc. Fig. 2 shows a root locus and highlights three configurations chosen for experiments. (a) tests the behavior of low damping ratio configurations. (b) shows borderline stable behavior. (c) confirms that vehicles with $M_u < 0$ are indeed unstable.

IV. EXPERIMENTS

A. Test Vehicle Design

The base of the test vehicle is a standard quadrotor stemming from a low cost design [9]. Although this specific vehicle has an IMU, an Invensense MPU-6050, its information is used for reporting purposes only. Unlike all other quadrotors, there is no active attitude controller running.

Rods are positioned at a distance such that stabilizers strung between them have a $5\,\mathrm{mm}$ clearance from the propellers, making the width of the stabilizers $0.135\,\mathrm{m}$ shown in Fig. 1. Despite this, we do not use any configurations that have material near the propellers to ensure that the stabilizers do not collide with the propellers during crashes and aggressive maneuvers. The placement also creates a cage, allowing for safe flight in cluttered environments. The stabilizers are $0.0005\,\mathrm{in}$ polyester film and cut with a laser cutter or vinyl cutter. We include tabs and slots on the ends of

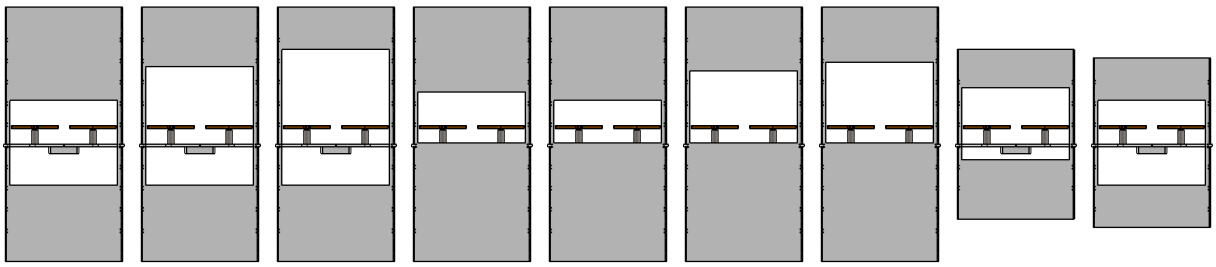

(a) (b) (c) (d) (e) (f) (g) (h) (i)

Fig. 3: Side-by-side comparison of the nine tested configurations

Quad	m	I_{YY}	d_1	d_2	d_3	d_4
	g	$\mathrm{g\,cm^2}$	m	m	m	m
(a)	39.6	1110	-0.16	-0.05	0.05	0.14
(b)	39.2	1070	-0.16	-0.09	0.05	0.14
(c)	39.0	1050	-0.16	-0.11	0.05	0.14
(d)	40.0	1120	-0.16	-0.06	0.00	0.14
(e)	40.1	1130	-0.16	-0.05	0.00	0.14
(f)	39.8	1100	-0.16	-0.85	0.00	0.14
(g)	39.7	1090	-0.16	-0.95	0.00	0.14
(h)	37.4	620	-0.11	-0.065	0.02	0.09
(i)	37.2	611	-0.10	-0.05	0.05	0.10

TABLE I: Tested vehicle configurations

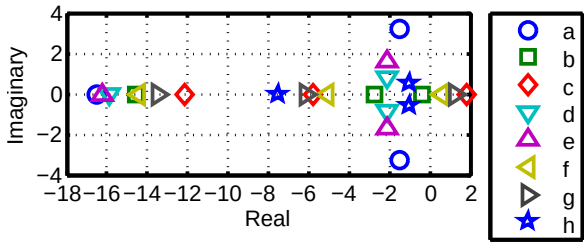

Fig. 4: Eigenvalues of the tested configurations

the sheet to make a loop. The design has slots for threading the rods through the stabilizer.

To find the flight envelope that is valid for the assumptions in Section II-B, we set a target mass of $40\,\mathrm{g}$. For that mass and a square duct of side length $0.135\,\mathrm{m}$, $\nu = 2.90\,\mathrm{m\,s^{-1}}$. The linear lift coefficient versus angle of attack assumption generally holds until stall, which usually occurs between $10°$ to $15°$. An angle of attack of $10°$ occurs at a horizontal velocity of $0.52\,\mathrm{m\,s^{-1}}$, which is 3.9 body lengths per second. The $\nu^2 + u^2 \approx \nu^2$ and $\arctan(\frac{u}{\nu}) \approx \frac{u}{\nu}$ assumptions result in 1.5% and 1.0% error respectively at this velocity, indicating their validity for this vehicle.

B. Vehicle Testing

We test numerous stabilizer configurations to verify that our analysis emulates the real world. Each configuration is placed on the ground in the center of a $3\,\mathrm{m}$ long by $3\,\mathrm{m}$ wide by $4\,\mathrm{m}$ tall room. A Vicon [10] motion capture system tracks the vehicle with a precision of $50\,\mu\mathrm{m}$ at up to $375\,\mathrm{Hz}$ [2]. A position and yaw controller runs off-board on a PC at $100\,\mathrm{Hz}$, which sends motor voltage commands to the vehicle. This differs from a traditional quadrotor where the position controller sends a desired vehicle attitude, and an inner attitude controller on-board the vehicle attempts to achieve it. Instead, we rely on the stabilizers to replace the inner attitude control loop.

Through position control, the quadrotor takes off and climbs to over $1.5\,\mathrm{m}$ from the ground. The x, y, and yaw controllers are then switched off, leaving only the z controller, causing all four motors to receive the same voltage commands. This condition emulates the math derived in Section II-A. Natural air currents perturb the vehicle.

We build nine configurations picked from the stability analysis to test the model validity at different points in the design space. The design parameters for each vehicle are listed in Table I. The predicted eigenvalues for these variants are shown in Fig. 4.

Designs (a), (b), and (c) are from the same family of stabilizers, all with a $0.3\,\mathrm{m}$ rod, $d_3 = 0.05\,\mathrm{m}$, and $d_4 = 0.14\,\mathrm{m}$. Essentially, we are trading between the sizes of the top stabilizer and the gap between the top stabilizer and the COM. Vehicle (a) has the lowest predicted damping ratio of this family and is exploring the practical limits of low damping ratios. Variant (b) is predicted to have the least stability while still remaining a stable configuration. Configuration (c) should have a COP $<$ COM, causing it to immediately fall over.

Like (a) through (c), vehicles (d) through (g) are also in their own family. These have a rod length of $0.3\,\mathrm{m}$, $d_3 = 0.00\,\mathrm{m}$, and $d_4 = 0.14\,\mathrm{m}$. Configuration (d) is predicted to be the most stable ($\min(\max(\mathrm{real}(\lambda))))$ vehicle of those with a rod length of $0.3\,\mathrm{m}$. Variant (e) has the lowest damping ratio of this family, and again is exploring the lower limit of damping ratios. Vehicle (f) is the closest unstable vehicle to being stable, while vehicle g is solidly unstable.

In general, it is desirable to use less material. Configuration (h) is predicted to be the most stable vehicle with a rod length of $0.2\,\mathrm{m}$, reducing the material used by a third. Variant (i) is a follow-up vehicle discussed in Section V-A.

C. Experimental Results

There are four easily identifiable cases of stability. The first is that the vehicle is stable and over-damped. This is characterized by a slow response and no oscillations. The eigenvalues of these vehicles are all negative real with no imaginary parts. We will label this case as $\lambda < 0, \zeta > 1$. We group critically damped vehicles in this category as cursory examination cannot discern the difference.

In the second case the vehicle is stable and under-damped, having a faster response, but also overshoots and oscillates.

Quad	Predicted λ vs 0	Predicted ζ vs 1	Actual λ vs 0	Actual ζ vs 1
(a)	$<$	$<$	$<$	$<$
(b)	$<$	$>$	$<$	$<$
(c)	$>$	$>$	$>$	$>$
(d)	$<$	$<$	$<$	$<$
(e)	$<$	$<$	$<$	$<$
(f)	$>$	$>$	$<$	$>$
(g)	$>$	$>$	$>$	$>$
(h)	$<$	$<$	$>$	$<$
(i)	$=$	$>$	$<$	$>$

TABLE II: Predicted and actual stability. Those that do not follow predictions are highlighted in red.

Their eigenvalues have negative real components, but also imaginary components. These are labeled $\lambda < 0$, $\zeta < 1$.

In the third case, the vehicle has a COP $<$ COM and the vehicle is unstable. The COP $<$ COM ($M_u < 0$) causes the vehicle to turn toward the direction of motion, and is the result of the bottom stabilizer dominating. These vehicles have positive real eigenvalues with no imaginary parts. Their labels are $\lambda > 0$, $\zeta > 1$, even though damping ratios are not typically used in unstable systems.

Finally, the forth case is when the vehicle has insufficient damping and is unstable. Here, the COP $>$ COM moment is too strong and the vehicle over-corrects, causing increasing oscillations. The eigenvalues are positive real with imaginary components. They are labeled as $\lambda > 0$, $\zeta < 1$.

Time series of some of the test flights are provided in Figures 5a to 5d. Actual values are those reported by a Vicon motion capture system. Desired values are the positions commanded by the position controller. In the beginning $2\,\mathrm{s}$ to $4\,\mathrm{s}$ of each time series the vehicle is flown to between $1.5\,\mathrm{m}$ to $2.5\,\mathrm{m}$ under full position control. When the x, y, and yaw controllers are switched off, the desired positions and the actual positions are the same.

Configuration (a) in Fig. 5a, chosen for exploring low damping ratios, behaves as expected. Both the x and y directions have $1.5\,\mathrm{s}$ oscillations which are very lightly damped, and close to the $1.77\,\mathrm{s}$ predicted by the eigenvalues. In gusty conditions, the light amount of damping may not be able to keep the vehicle upright.

Vehicle (b) in Fig. 5b is less damped than expected. It is predicted to be over-damped, but is actually lightly under-damped with an oscillation period of $4\,\mathrm{s}$.

Variant (c) in Fig. 5c shows the x and y velocities growing to the limits of the room with no oscillations. This is characteristic of COP $<$ COM. Interestingly, the position controller is sufficient to stabilize this vehicle during climb, indicating that it is only slightly unstable as predicted.

Configuration (d) in Fig. 5d, chosen for its fast and lightly under-damped response time, behaves as expected. The $2.25\,\mathrm{s}$ oscillations are heavily damped and are very close to the predicted period of $2.76\,\mathrm{s}$. The horizontal velocities do not grow beyond $0.35\,\mathrm{m\,s^{-1}}$.

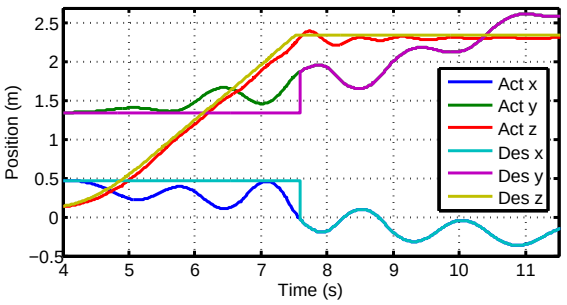

(a) Configuration a: stable but very under-damped.

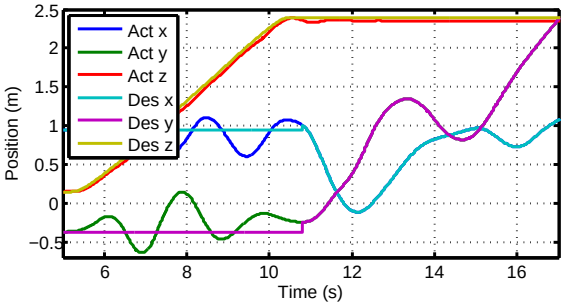

(b) Configuration b: stable and lightly under-damped.

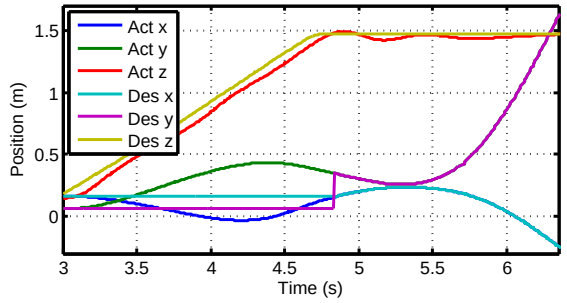

(c) Configuration c: unstable and fails the $M_u > 0$.

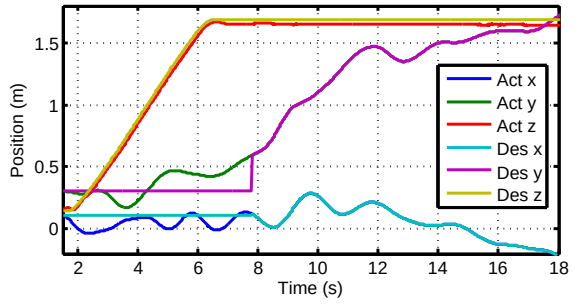

(d) Configuration d: stable, lightly under-damped, and demonstrates the desired response.

Fig. 5: Test flights of configurations (a),(b),(c), and (d)

V. DISCUSSION

A. Theory Verification

The majority of experiments are consistent with theory. Five of the nine configurations behave as expected. When the vehicles are predicted to be under-damped, their oscillation periods are similar, yet all are lower than predicted. This is potentially explained by the lack of an X_q term in the model.

Three of the first eight experiments do not match theory. All three show a push towards more negative reals, then more imaginary eigenvalues. This is characteristic of less damping than expected, and can happen if either the top stabilizer produces more lift and/or the bottom stabilizer produces less lift than expected. The inflow, described in Section II-B, around an unobstructed rotor contracts in its wake. One possible explanation that the airflow contracts below the quadrotor's propellers, creating a high velocity channel of

What	Crazyflie	Ladybird V1	Passive 1	Passive 2
Retail $	116.00	89.00	-	-
μc	32F103CB	XMEGA16D4	32F373CB	ATtiny9
μc $	2.82	0.97	2.47	0.39
Accel	MPU-6050	ITG-3205	None	None
Accel $	4.62	3.67	0.00	0.00
Gyro	MPU-6050	MMA8452Q	None	None
Gyro $	(4.62)	0.73	0.00	0.00
Passive $	-	-	3.54	0.24
Total	7.44	4.64	6.01	0.63

TABLE III: Vehicle costs for a run of 1000 in USD

air between the stabilizers and less airflow near them. This suggests the β adjustment term should be different for the top and bottom stabilizers. If this is the case, a vehicle with an even distribution of stabilizers above and below the COM should have a COP $>$ COM. We use the follow-up vehicle, (i), shown in Fig. 1 to test this idea. This configuration is indeed stable, but has a large bounded linear velocity.

Another observation is that when the controllers turn off, all of the vehicles move in the negative x and positive y directions. In fact, a close look at Fig. 5c shows that the vehicle even changes direction when the controllers turn off. This is consistent with either an unbalanced vehicle in either thrust or mass distribution, which favors one side of the vehicle versus another, or the wind in that location of the room is higher than vehicle (c)'s speed.

The main goal of this analysis is to provide a tool for finding quality configurations analytically or numerically, not experimentally. Configuration (d) is the result of this search for our quadrotor. With this set of stabilizers, the vehicle is not only stable without an attitude controller, but is capable of following trajectories like any other quadrotor. Furthermore, it is robust to large wind gusts and crashes.[1]

B. Vehicle Cost

One of the main advantages of a passively stabilized MAV is its reduction in cost. In Table III we see the cost of the stabilizing components of three actual and one theoretical quadrotor of similar size: the Bitcraze Crazyflie, Walkera Ladybird V1, our passive quadrotor, and a cost optimized passive quadrotor. For a fair comparison, all products were reverse engineered and component costs are listed for production runs of 1000[2]. Not only can we remove the accelerometer and gyroscope from the passive quadrotor, but the microcontroller no longer estimates attitude and controls. A simpler and lower cost microcontroller only reads voltage commands from the radio and outputs them on four PWMs.

The added components are the four rods, assumed to be $0.3\,\mathrm{m}$ each, and $4\times0.3\,\mathrm{m}\times0.135\,\mathrm{m} = 0.162\,\mathrm{m}^2$ of film. The rods cost $2.62\,\$/\mathrm{m}$ and film costs $2.34\,\$/\mathrm{m}^2$. This leaves the added cost of the passive mechanism to be $4 \times 0.3 \times 2.62 + 0.162 \times 2.34 = \$3.52$, which on par with the cheapest quadrotors' electronics and without any cost optimization. Replacing the carbon fiber rods with birch wood at $0.23\,\$/\mathrm{m}$ and the polyester film with polyethylene at $0.09\,\$/\mathrm{m}^2$ the cost is merely \$0.24. Thus, passive stability can save nearly an order of magnitude on control costs.

[1] See accompanying video for trajectory following and perturbation demo.

[2] Prices from Octopart, McMaster-Carr, and Dragonplate on Feb. 26, 2015

C. Efficiency Effects

To fly, aerial vehicles must support their own weight, so the vehicle's mass is a critical design constraint. Although we can remove the accelerometer and gyroscope, the mass of the vehicle is not significantly reduced. The base quadrotor weighs $33\,\mathrm{g}$, while the configurations with $0.3\,\mathrm{m}$ rods weigh roughly $40\,\mathrm{g}$, which requires 21% more thrust for hover.

Assuming the translational drag on the quadrotor itself remains the same, the added thrust required to move linearly can be derived from X_u. The horizontal force $F = mX_u u$. As mentioned in Section IV-A, the linear assumptions hold up to $0.52\,\mathrm{m\,s^{-1}}$ and perhaps faster depending on the onset of stall. Of the configurations with a rod length of $0.3\,\mathrm{m}$, the average predicted $\bar{X_u} = -3.98$, resulting in the added thrust requirement of $F = 3.98 \times 0.04u = 0.159u\mathrm{N}$. For example, the hover thrust of our vehicle is $mg = 0.04 \times 9.81 = 0.392\mathrm{N}$ and the linear drag force moving at $0.5\,\mathrm{m\,s^{-1}}$ is $F = 0.159 \times 0.5 = 0.080\mathrm{N}$. So, the required thrust to translate is $\sqrt{(mg)^2 + F^2} = 0.401\mathrm{N}$, a 2.1% increase.

VI. CONCLUSION

In this paper, we analyzed the effects of lifting stabilizers, predicted their stabilizing traits, confirmed the analysis by building flying vehicles, and reviewed some benefits and drawbacks. Throughout the analysis new and interesting problems arose. The cause of the over-prediction of the bottom stabilizer's force or the under-prediction of the top stabilizer's force remains an open problem. A similar analysis on yaw may provide useful as the vehicle currently has no controller in this direction. Perhaps most interesting is when these vehicles stop creating thrust while in flight, they rotate horizontally and glide safely and slowly toward the ground. Future vehicles should incorporate these unexplored features for even safer and more stable MAVs.

REFERENCES

[1] P.Pounds *et al.*, "Modelling and control of a quad-rotor robot," in *Proceedings Australasian Conference on Robotics and Automation 2006*. Australian Robotics and Automation Association Inc., 2006.

[2] N.Michael *et al.*, "The grasp multiple micro-uav testbed," *Robotics & Automation Magazine, IEEE*, vol. 17, no. 3, pp. 56–65, 2010.

[3] S.Bouabdallah, "Design and control of quadrotors with application to autonomous flying," Ph.D. dissertation, École Polytechnique federale de Lausanne, 2007.

[4] I.Sadeghzadeh *et al.*, "Fault-tolerant trajectory tracking control of a quadrotor helicopter using gain-scheduled pid and model reference adaptive control," in *Annual Conference of the Prognostics and Health Management Society*, vol. 2, 2011.

[5] M.Piccoli and M.Yim, "Passive stability of a single actuator micro aerial vehicle," in *Robotics and Automation (ICRA), 2014 IEEE International Conference on*. IEEE, 2014, pp. 5510–5515.

[6] Z. E.Teoh *et al.*, "A hovering flapping-wing microrobot with altitude control and passive upright stability," in *Intelligent Robots and Systems (IROS), 2012 IEEE/RSJ International Conference on*. IEEE, 2012, pp. 3209–3216.

[7] F.vanBreugel *et al.*, "From insects to machines," *Robotics & Automation Magazine, IEEE*, vol. 15, no. 4, pp. 68–74, 2008.

[8] G. D.Padfield, *Helicopter flight dynamics*. John Wiley & Sons, 2008.

[9] A.Mehta *et al.*, "A scripted printable quadrotor: Rapid design and fabrication of a folded mav," in *16th International Symposium of Robotics Research (ISRR13)*, 12 2013.

[10] Vicon, "Vicon systems," 9 2014. [Online]. Available: http://www.vicon.com/System/TSeries